

Article

Dynamic Non-Destructive Evaluation of Piezoelectric Materials to Verify on Accuracy of Transversely Isotropic Material Property Measured by Resonance Method

Yu-Hsi Huang ^{1,*} , Chien-Yu Yen ¹ and Tai-Rong Huang ²

¹ Department of Mechanical Engineering, National Taiwan University, Taipei 10617, Taiwan; d08522007@ntu.edu.tw

² Taiwan Semiconductor Manufacturing Company, Hsinchu 30078, Taiwan; nilson444@yahoo.com.tw

* Correspondence: yuhsih@ntu.edu.tw; Tel.: +886-233662690

Received: 23 June 2020; Accepted: 21 July 2020; Published: 23 July 2020



Featured Application: This paper provides the measurement methods and corresponding calculating formulas for piezoelectric material constants. The completely orthotropic material property, i.e., dielectric, piezoelectric, and elastic constants, is obtained and verified by piezoelectric dynamic characteristics. By means of use in anisotropic material property, the mode shape and corresponding natural frequency were determined by finite element numerical calculation. The difference is rare in comparison with the results obtained by optically dynamic vibration measurement. The influence on self-heating phenomenon of soft and hard piezoelectric ceramics is also discussed in the study.

Abstract: In many engineering applications of piezoelectric materials, the design and prediction of the dynamic characteristics depends on the anisotropic electromechanical material property. Through collecting the complete formula in literature and listing all the prepared specimens, transversely isotropic material constants were obtained and verified by dynamic non-destructive evaluation in the paper. The IEEE (Institute of Electrical and Electronics Engineers) resonance method was applied to measure and calculate the orthotropic material constants for piezoelectric ceramics. Five specimens need to be prepared for the measurements using an impedance analyzer, in order to obtain the resonant and anti-resonant frequencies from the modes of thickness extension, length-extension, thickness-shear extension, length-thickness extension, and radial extension. The frequencies were substituted into the formulas guided on the IEEE standard to determine the elastic, dielectric, and piezoelectric constants. The dynamic characteristics of soft and hard piezoelectric ceramics in the results from the finite element method (FEM), which is analyzed from the anisotropic material constants of the resonance method, were verified with the mode shapes and natural frequencies found by experimental measurements. In self-heating, considered as operating on resonant frequencies of piezoelectric material, the resonant frequency and corresponding mode shape calculated by the material constants from resonance method in FEM are more accurate than the material property provided by the manufacturer and literature. When the wide-bandwidth frequency is needed to design the application of piezoelectric ceramics, this study completely provided the measurement method and dynamic verification for the anisotropic electromechanically material property.

Keywords: piezoelectric materials; transversely isotropic material; IEEE resonance method; resonant and anti-resonant frequencies; dynamic non-destructive evaluation

1. Introduction

Piezoelectric materials are smart materials which serve as crucial components in sensors or actuators. When the need arises for vibration control in lightweight flexible structures with complex shapes, piezoelectric sensors and actuators can be used to prevent adding to the overall mass of the structure and to achieve precision control. Piezoelectric materials have superior electromechanical properties, are lightweight and easy and inexpensive to produce, and have low power consumption [1–4]. For instance, the puncture systems used in cellular biology research have precise and fine vibration control [5]. In addition to applying the vibration characteristics of inverse piezoelectricity, the puncture systems also apply energy extraction systems with direct piezoelectric effects. Recently, vibration energy harvesting devices using piezoelectric materials have garnered the attention of researchers. These devices convert the vibration energy of mechanical structures into usable electrical energy, which can detect the inhibiting effects of vibration signals [6]. Energy harvesting systems based on lead zirconate titanate (PZT) can be embedded into vibrating objects to generate tens to hundreds of microwatts of energy for low-power integrated circuits (ICs). Thus, piezoelectric materials can be combined with low-power ICs to create continuously-working miniature wireless sensors, such as implantable biomedical sensors and wearable devices [7], wireless sensor networks [8], and smart buildings and special structures [9–11]. The vibration characteristics of piezoelectric materials can be analyzed in advance using finite element software for greater convenience in the optimization of piezoelectric effects. To obtain accurate analysis results, the boundary conditions of the model must be clearly defined, and the right piezoelectric material parameters must be used. The parameters provided with commercially-available piezoelectric materials are often inadequate for numerical calculations. Complete dynamic characteristics cannot be derived from the mechanical parameters of anisotropic materials, and thus, measuring effective and complete material parameters is key to analysis accuracy.

In this study, the material constants of the piezoelectric specimens were measured using the resonance method (RM). This method has been widely applied. In 1954, Mason et al. [12] used the resonance characteristics of an equivalent circuit simulating a piezoelectric crystal and employed static methods, quasi-static methods, dynamic methods, and hydrostatic methods to measure the elastic, piezoelectric, and dielectric constants of 45° Rochelle salt. Based on these measurement methods, they then developed RM to measure the material properties of piezoelectric crystals. In this method, the elastic and piezoelectric constants of the piezoelectric crystal are measured and the dielectric constants are inversely calculated from measured capacitance. Although the compliance S_{11}^E and S_{11}^D , electromechanical coupling coefficients k_{33} and k , and permittivity ϵ_{33}^T were obtained, the measurement was lack of guideline for prepared the standard specimens. In 1961, the IRE Standards on Piezoelectric Crystals [13] presented five specimens with different geometric shapes, aspect ratios, polarization orientations, and electrode surface orientations. The mode shapes corresponding to these five specimens were the thickness extension (TE) mode, length extension (LE) mode, thickness shear extension (TS) mode, length thickness extension (LTE) mode, and radial extension (RAD) mode. As polarized PZT has a hexagonal lattice (6 mm), it has 10 material constants, including five elastic constants, three piezoelectric constants, and two dielectric constants. With the TE, LE, TS, LTE, and RAD modes, the resonant and anti-resonant frequencies can be measured, and then the material constants of its various forms can be inversely calculated.

In 1987, the IEEE (Institute of Electrical and Electronics Engineers) Standards [14] referred to the RM in the IRE Standards and established a complete resonance measurement method with complete assumptions regarding constitutive equations (d-form, e-form, g-form, and h-form) and simplified specimen dimensions for piezoelectric materials and five specimens with different geometric shapes, aspect ratios, polarization orientations, and electrode surface orientations. Some formula listed in Refs [13,14] are more complicated, therefore the simplified form was proposed by subsequent researcher. In 1989, Wang et al. [15] applied the thickness vibration theory in RM to the vibrations in a piezoelectric plate in which the length and width are assumed to be much greater than the thickness that they approach infinity. They used α -quartz with two different cuts to measure the elastic, piezoelectric, and

dielectric constants of α -quartz. The material constants of Y-cut quartz were studied in the paper; hence, the method is not provided for obtained the complete transversely piezoelectric isotropic material constants. In 1998, Cao et al. [16] conducted a detailed study on specimens with two types of shear mode shapes: thickness shear and length shear. They examined specimens with different aspect ratios and compared their measurements. The experiment results revealed that only the length-to-thickness ratio has a direct relationship and influences the values of the resonant and anti-resonant frequencies. A pure shear mode shape can be generated at $l/20t$, thereby reducing the errors in the resonant and anti-resonant frequency measurements.

We used an impedance analyzer to measure the resonant and anti-resonant frequencies of piezoelectric materials and substituted them into the equations listed in RM to obtain 10 independent material constants. Although the material parameters of piezoceramics are practically independent from frequency in the order of several MegaHertz [17–19], in the frequencies of the order of kilohertz—several tens of kilohertz—the dependence on frequency is very strong. It performs on the main resonances in longitudinal, transverse, shear, or radial modes. We then substituted the measured material constants into finite element numerical calculations to verify the in-plane and out-of-plane resonant frequencies and mode shapes of the piezoelectric materials. The experimental measurements of the out-of-plane resonant frequencies and mode shapes were obtained using electronic speckle pattern interferometry (ESPI), whereas the in-plane vibrations were measured using ESPI and an impedance analyzer. A comparison of the experiment results and the numerical calculations revealed fairly good accuracy in the material constants obtained using RM.

2. Theory Based on Resonance Method

From the linearly electro-thermo-elastic model [20], the constitutive equations are represented as

$$T_{ij} = c_{ijkl}S_{kl} - e_{ijk}E_k - \alpha_{ij}\theta \tag{1}$$

$$D_i = e_{ijk}S_{kl} + \varepsilon_{ij}^S E_j - \lambda_i \theta \tag{2}$$

$$\eta = \alpha_{kl}S_{kl} + \lambda_k E_k + C_\theta \theta \tag{3}$$

$$q_i = -K_{ij}\theta_{,j} \tag{4}$$

In these equations, T_{ij} , S_{kl} , E_k , D_i , q_i and θ are the components of stress, strain, electric field, electric displacement, heat flux and temperature difference with initial condition, respectively. The c_{ijkl} , e_{ijk} , α_{ij} , ε_{ij}^S , λ_i , C_θ and K_{ij} are the components of elastic, piezoelectric, thermal expansion, permittivity, pyroelectric coefficients, and the thermal conductivity tensor, respectively. If neglecting the thermo-elastic and thermo-electrical effects, the piezoelectric e -form is

$$\begin{cases} T_{ij} = c_{ijkl}S_{kl} - e_{ijk}E_k \\ D_i = e_{ijk}S_{kl} + \varepsilon_{ij}^S E_j \end{cases} \tag{5}$$

and the d -form constitutive equations are, respectively,

$$\begin{cases} S_{ij} = s_{ijkl}T_{kl} + d_{kij}E_k \\ D_i = d_{ikl}T_{kl} + \varepsilon_{ik}^T E_k \end{cases} \tag{6}$$

The linear piezoelectric constitutive equations for a piezoceramic material with crystal symmetry class C_{6mm} are presented in the components of elastic (c_{pq}^E), piezoelectric (e_{pq}), and dielectric coefficients (ε_{pq}^S) respectively.

The IEEE Standards [14] indicate that measuring the complete material constants of piezoelectric ceramic material requires piezoelectric specimens with five different mode shape characteristics (TE, LE, TS, LTE, and RAD), each with its own geometric shape, aspect ratio, polarization orientation,

and electrode surface orientation. We used an impedance analyzer (model: HP-4194A) to measure their resonant and anti-resonant frequencies and inversely calculate the material constants of the piezoelectric materials. Based on Equations (7), (8), (12), (13), (19), (20), (22), and (23), the characteristics of the impedance measurements for TE, LE, TS, and LTE are as shown in Figure 1. Only one set of resonant and anti-resonant frequency values (f_r , f_a) needs to be substituted into Equations (25) and (26). In Equations (25) and (26) for RAD, the impedance measurement characteristics, as shown in Figure 1, have two sets of resonant and anti-resonant frequency values (f_1^r , f_1^a , f_2^r , f_2^a). Below, we obtain the material constants from the specimens of the five vibration modes according to the explanations in Ref [14].

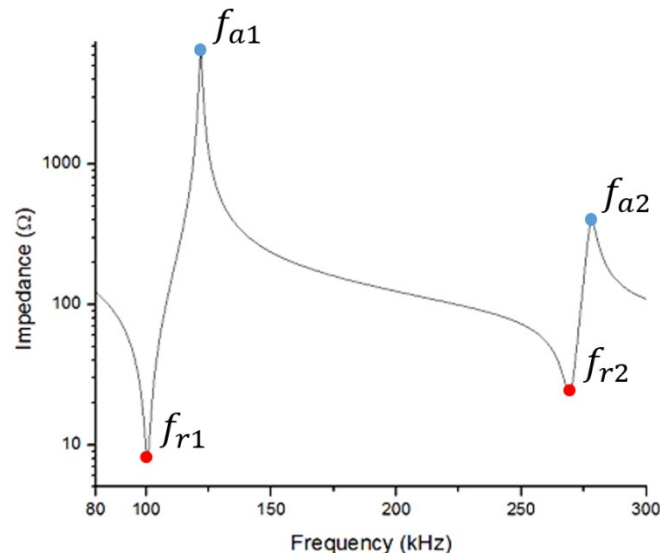


Figure 1. Schematics in resonant and anti-resonant frequencies obtained by impedance analyzer.

2.1. Thickness Extension (TE)

Table 1 presents the geometric shape and material constants of a thin square plate in which the directions of polarization and vibration are oriented along the depth (thickness). When the aspect ratios of the component satisfy $l > 10t$ and $w > 10t$, we use five specimens with dimensions $l = 46 \pm 0.1$ mm, $w = 46 \pm 0.1$ mm, and $t = 1.2$ mm, and the following equations can be used to calculate their material constants:

$$k_t^2 = \frac{\pi f_r}{2 f_a} \cot\left(\frac{\pi f_r}{2 f_a}\right) \tag{7}$$

$$c_{33}^D = 4\rho(t f_a)^2 \tag{8}$$

$$c_{33}^E = c_{33}^D(1 - k_t^2) \tag{9}$$

where k_t is the electromechanical coupling coefficient by thickness extension mode, f_r is resonant frequency, f_a is anti-resonant frequency, t is the thickness of specimen, and ρ is the density of specimen.

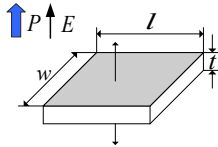
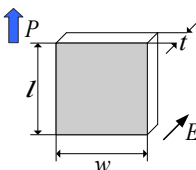
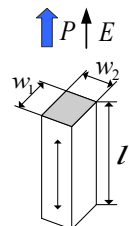
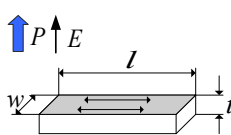
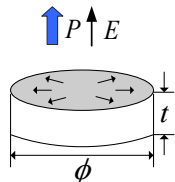
For the dielectric constant, the capacitance measured using an impedance analyzer at a specific frequency (1 kHz) can be substituted into the following equations, which will produce ϵ_{33}^T , the dielectric constant in constant stress, and ϵ_{33}^S , the dielectric constant in constant strain:

$$\epsilon_{33}^T = \frac{C_l \cdot t}{A} \tag{10}$$

$$\epsilon_{33}^S = \frac{C_h \cdot t}{A} \tag{11}$$

where A is the area of the electrode, C_l is the capacitance under 1kHz, and C_h is the capacitance at twice the anti-resonant frequency ($2f_a$).

Table 1. Specification on vibration modes of standard piezoelectric elements and their correspondent measured material constants [14].

Mode	Specification	Obtained Material Constant			
		k	d	s^E	ϵ^T
Thickness Extension (TE)	 <p>$l > 10t, w > 10t$</p>	k_t	d_{33}	s_{33}^E	ϵ_{33}^T
Thickness Shear Extension (TS)	 <p>$l > 20t, w > 10t$</p>	k_{15}	d_{15}	s_{44}^E	ϵ_{11}^T
Length Extension (LE)	 <p>$l > 5w_1, w > 5w_2$</p>	k_{33}	d_{33}	s_{33}^E	ϵ_{33}^T
Length Thickness Extension (LTE)	 <p>$l > 10t, l > 3w, 3t > w$</p>	k_{31}	d_{31}	s_{11}^E	ϵ_{33}^T
Radial Extension (RAD)	 <p>$\phi > 20t$</p>	k_p	d_{31}	s_{11}^E	ϵ_{33}^T

E: Electric-field direction; P: Polarization direction.

2.2. Thickness Shear Extension (TS)

In this mode, we have a thin square plate in which the polarization is oriented along the length, and shear vibrations occur along the depth. In other words, the orientation of polarization is perpendicular to the direction of the electric field, causing the piezoelectric component to display shear vibrations. Table 1 presents the geometric shape and material constants. When the aspect ratios of the component

satisfy $l > 20t$ and $w > 10t$, we use five specimens with dimensions $l = 9 \pm 0.05$ mm, $w = 8 \pm 0.05$ mm, and $t = 0.52$ mm, and the following equations can be used to calculate their material constants:

$$k_{15}^2 = \frac{\pi f_r}{2 f_a} \cot\left(\frac{\pi f_r}{2 f_a}\right) \tag{12}$$

$$c_{44}^D = 4\rho(t f_a)^2 \tag{13}$$

$$c_{44}^E = c_{44}^D(1 - k_{15}^2) \tag{14}$$

For PZT material, the following relations can be used to derive S_{44}^D , the elastic compliance constant with constant electric displacement, and S_{44}^E , the elastic compliance constant in a constant electric field:

$$S_{44}^D = 1/c_{44}^D \tag{15}$$

$$S_{44}^E = 1/c_{44}^E \tag{16}$$

where k_{15} is the electromechanical coupling coefficient of the thickness shear mode shape.

For the dielectric constant, the capacitance measured using an impedance analyzer at a specific frequency (1 kHz) can be substituted into the following equations, which will produce ϵ_{11}^T , the dielectric constant in constant stress, and ϵ_{11}^S , the dielectric constant in constant strain:

$$\epsilon_{11}^T = \frac{C_L \cdot t}{A} \tag{17}$$

$$\epsilon_{11}^S = \frac{C_H \cdot t}{A} \tag{18}$$

C_L is the capacitance measured at 1 kHz, and C_H is the capacitance measured at twice the anti-resonant frequency ($2f_a$).

2.3. Length Extension (LE)

In this mode, we have a thin square column in which the polarization and vibrations are oriented along the direction of the length. Table 1 presents the geometric shape and material constants. When the aspect ratios of the component satisfy $l > 5w_1$ and $w > 5w_2$, we use five specimens with dimensions $l = 10 \pm 0.1$ mm, $w_1 = 1.4 \pm 0.1$ mm, and $w_2 = 0.51$ mm, and the following equations can be used to calculate their material constants, where k_{33} denotes the electromechanical coupling coefficient of the longitudinal length mode shape, and l is the length of specimen.

$$k_{33}^2 = \frac{\pi f_r}{2 f_a} \cot\left(\frac{\pi f_r}{2 f_a}\right) \tag{19}$$

$$S_{33}^D = \frac{1}{4\rho(l f_a)^2} \tag{20}$$

$$S_{33}^E = \frac{S_{33}^D}{1 - k_{33}^2} \tag{21}$$

2.4. Length Thickness Extension (LTE)

In this mode, we have a thin square plate in which the polarization is oriented along the depth and lateral vibrations occur along the length. In other words, the vibrations occur along the length and perpendicular to the polarization orientation. Table 1 presents the geometric shape and material constants. When the aspect ratios of the component satisfy $l > 10t$, $l > 3w$, and $3t > w$, we use five

specimens with dimensions $l = 31.8 \pm 0.1$ mm, $w = 3 \pm 0.1$ mm, and $t = 1.21$ mm, and the following equations can be used to calculate their material constants:

$$\frac{k_{31}^2}{k_{31}^2 - 1} = \frac{\pi f_a}{2 f_r} \cot\left(\frac{\pi f_a}{2 f_r}\right). \tag{22}$$

$$S_{11}^E = \frac{1}{4\rho(lf_r)^2} \tag{23}$$

$$S_{11}^D = S_{11}^E(1 - k_{31}^2) \tag{24}$$

where k_{31} denotes the electromechanical coupling coefficient of the thickness shear mode shape.

2.5. Radial Extension (RAD)

In this mode, we have a thin round plate in which the polarization and vibrations are both oriented along the depth. Table 1 presents the geometric shape and material constants. The aspect ratios of the component must satisfy $\varnothing > 20t$, and we use five specimens with dimensions $\varnothing = 19.9 \pm 0.05$ mm and $t = 0.81$ mm. In 1973, Meitzler, O’Bryan, and Tiersten [21] derived the constants of radial vibrations in round plates. The formula for k_p , the electromechanical coupling coefficient of the radial vibrations in a piezoelectric round plate is

$$\frac{k_p^2}{1 - k_p^2} = \frac{(1 - \sigma^E)J_1[\eta_1(1 + Hf/f_r)] - \eta_1(1 + \Delta f/f_r)J_0[\eta_1(1 + \Delta f/f_r)]}{(1 - \sigma^E)J_1[\eta_1(1 + \Delta f/f_r)]} \tag{25}$$

where k_p denotes the electromechanical coupling coefficient of the radial mode shape; $\Delta f = f_a - f_r$ is the difference between the anti-resonant frequency and the resonant frequency; J_0 is Bessel Function of First Kind and Zero Order; J_1 is Bessel Function of First Kind and First Order; σ^E is Poisson’s Ratio; and η_1 is the first positive root from the function $(1 - \sigma^E)J_1(\eta) = \eta J_0(\eta)$. However, in 2005, Zhang, Alberta, and Eitel [22] modified the electromechanical coupling relation above using approximation into

$$k_p^2 = \frac{1}{P} \cdot \frac{f_a^2 - f_r^2}{f_a^2} \tag{26}$$

where

$$P = \frac{2(1 + \sigma^E)}{\{\eta_1^2 - [1 - (\sigma^E)^2]\}} \tag{27}$$

Based on RM by IEEE standard [14,15], several formula were simplified also by Zhang et al. [22] and we used them to calculate some parameters, i.e., ε_{33}^T , ε_{33}^S , ε_{11}^T .

RM uses the vibration characteristics corresponding to the five types of piezoelectric components above to derive the elastic, piezoelectric, and dielectric constants. Furthermore, Poisson’s ratio is defined as the ratio of lateral strain to longitudinal strain:

$$\sigma^E = -\frac{S_{12}^E}{S_{11}^E} \tag{28}$$

where the superscript E indicates values measured in a fixed electric field. The negative indicates that the two vibrations are opposite in direction, which means that when the longitudinal vibration is extending, the lateral vibration is contracting, and when longitudinal vibration is contracting, the lateral vibration is extending. Obtaining the Poisson’s ratio generally requires the measurement of the fundamental frequency and one overtone frequency of the piezoelectric round plate. The formula used is $(1 - \sigma^E)J_1(\eta) = \eta J_0(\eta)$, the source and usage of which are explained in Ref [23,24]. Then, η_1 and η_2

are calculated, and we can look up the fundamental frequency $f_r = f_1^r$ and the overtone frequency f_2^r in the table provided in the Appendix to determine the Poisson's ratio σ^E , which is substituted into Equation (25) to derive k_p , the electromechanical coupling coefficient of the radial mode shape.

Although RM can be used to obtain the material constants of piezoelectric materials, there are still some constants that cannot be measured via experiment, and some conversions between constants are required to derive the constants that cannot be directly measured before all of the elastic, piezoelectric, and dielectric constants are obtained. Below is the solved equation including the piezoelectric strain constant:

$$d_{ij}^2 = k_{ij}^2 \varepsilon_{ii}^T s_{jj}^E \tag{29}$$

where $ij = 31, 33, 15$. Based on the equation above, if k_{ij} , ε_{ij}^T , and s_{ij}^E (i.e., the electromechanical coupling coefficient, the dielectric constant in constant stress, and the elastic compliance constant in a constant electric field) are known, then d_{31} , d_{33} , and d_{15} , (i.e., the piezoelectric strain constants) can be obtained. Next, we can use the following equations to obtain the other elastic and compliance constants:

$$s_{12}^E = -\sigma^E \cdot s_{11}^E \tag{30}$$

$$s_{12}^D = s_{12}^E - k_{31}^2 \cdot s_{11}^E \tag{31}$$

$$s_{66}^E = s_{66}^D = \frac{1}{c_{66}^E} = \frac{1}{c_{66}^D} = 2(s_{11}^E - s_{12}^E) \tag{32}$$

$$s_{13}^D = -\left\{ \frac{s_{11}^D + s_{12}^D}{2} \cdot \left(s_{33}^D - \frac{1}{c_{33}^D} \right) \right\}^{0.5} \tag{33}$$

$$s_{13}^E = s_{13}^D + k_{31} \cdot k_{33} (s_{33}^E \cdot s_{11}^E)^{0.5} \tag{34}$$

$$c_{11}^E = \frac{s_{11}^E s_{33}^E - (s_{13}^E)^2}{(s_{11}^E - s_{12}^E) \left[s_{33}^E (s_{11}^E + s_{12}^E) - 2(s_{13}^E)^2 \right]} \tag{35}$$

$$c_{12}^E = \frac{-s_{12}^E s_{33}^E + (s_{13}^E)^2}{(s_{11}^E - s_{12}^E) \left[s_{33}^E (s_{11}^E + s_{12}^E) - 2(s_{13}^E)^2 \right]} \tag{36}$$

$$c_{13}^E = \frac{-s_{13}^E}{s_{33}^E (s_{11}^E + s_{12}^E) - 2(s_{13}^E)^2} \tag{37}$$

Using Equations (30) through (37), we can obtain all of the elastic and compliance constants. We can then use $\varepsilon_{ik}^T = \varepsilon_{ik}^S + d_{ip} e_{kp}$ to obtain the piezoelectric stress constant e_{ij} . The primary calculation formulas are as follows:

$$e_{31} = d_{31} (c_{11}^E + c_{12}^E) + d_{33} c_{13}^E \tag{38}$$

$$e_{33} = 2d_{31} c_{12}^E + d_{33} c_{33}^E \tag{39}$$

$$e_{15} = d_{15} c_{44}^E \tag{40}$$

3. Specimens and Experimental Techniques

This study performed the experimental measurements and material constant calculations of two piezoelectric ceramic materials using RM. The in-plane and out-of-plane vibration characteristics were measured using instruments to verify the accuracy of the material constants obtained using finite element analysis. Below, we introduce the piezoelectric materials and instruments used in this study.

3.1. Preparation on Piezoelectric Ceramics

To establish complete piezoelectric ceramic material constants, we used RM to perform measurements of five specimens with specific geometric shapes, aspect ratios, polarization orientations, and electrode surface orientations. As shown in Table 1, the specific mode shapes include the TE, LE, TS, LTE, and RAD modes.

We procured piezoelectric ceramic specimens that fit the specifications of the TE and RAD modes in RM from American Piezo Ceramics (APC) International, Ltd. and the Fuji Ceramics Corporation. The piezoelectric specimens for the LE and LTE modes were cut to the required aspect ratios using ultrasonic cutting. Finally, for the TS mode, we ground our own specimen, removed the electrodes, and redistributed the electrodes in the direction normal to that of polarization so that the aspect ratio, polarization orientation, and the direction of the electric field created by the electrodes would meet specifications for TS mode testing.

3.2. Impedance Analysis

We derived material constants using the theoretical equations in RM. The resonant and anti-resonant frequencies substituted into the equations were obtained by measuring the mode shapes with specific structures, namely the TE, LE, TS, LTE, and RAD modes, using an impedance analyzer.

An impedance analyzer uses fixed voltages to excite vibrations in the target object and then measures the continuous changes in electrical impedance at various frequencies, as shown in Figure 1. The electrical impedance can be regarded as the total impedance applied by the resistors, inductors, and capacitors in the target object on the alternating current. Coupling characteristics are evident in the conversion between electrical and mechanical energy in piezoelectric materials. Thus, the electrical impedance of piezoelectric materials differs from that of components without piezoelectric properties. Generally, the results will display a resonant frequency ($f_{resonance}$, f_r) or anti-resonant frequency ($f_{anti-resonance}$, f_a) at certain resonant frequencies in frequency-impedance characteristic diagrams.

3.3. Electronic Speckle Pattern Interferometry (ESPI)

We input the material constants derived from measurements and calculations using RM and the material parameters provided by manufacturers or literature into finite element software to analyze vibration characteristics and obtain resonant frequency values and mode shapes. Next, we used the vibration characteristics obtained using optical non-destructive testing to verify the accuracy of RM.

Derived from holography, ESPI involves the casting of two coherent light beams on the target object and then the differences and changes in the optical path lengths are used to obtain the deformation data of the target object. The measurement method commonly used when ESPI is applied to vibrations is the time-averaging method. Within the exposure time of the CCD (charge-coupled device), images of the vibrating object are captured at different times, and a zero-order Bessel function is used to modulate the interference fringes. The brightest region in the interference images is the nodal line, where the displacement is zero, and the light and dark fringes show the contours of displacement. The resolution of the measurement system depends on the light source wavelength. We set up a sub-micron level ESPI system so as to obtain the full-field distributions of micro-vibration displacements in the interference patterns [25,26]. We then compared the ESPI measurement results of the low-frequency out-of-plane vibrations and the high-frequency in-plane vibrations in the piezoelectric specimens with the FEM analysis results derived from the piezoelectric material constant inputs.

3.3.1. Out-Of-Plane Vibration

As shown in Figure 2, a beam splitter is used to create two coherent laser beams. The one applied to the object surface is the object beam, whereas the other, known as the reference beam, is projected on a reference plate so that it scatters to create a speckled image. The two coaxial beams reflect and focus on the photosensitive plane of a CCD camera and create interference images. Using differencing

calculations to process the images then swiftly produces interference fringe patterns on the computer screen, thereby providing real-time measurements during experiments.

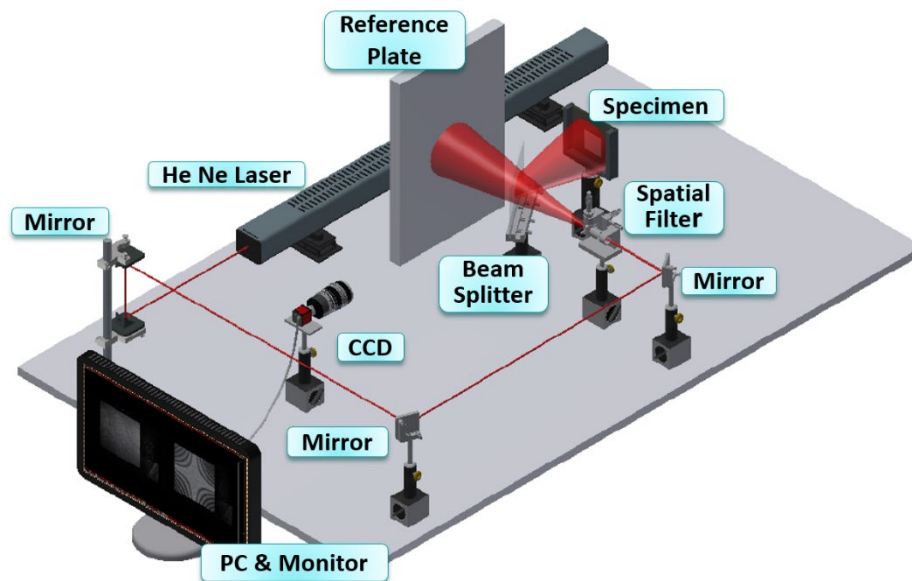


Figure 2. Out-of-plane setup in ESPI.

3.3.2. In-Plane Vibration

As shown in Figure 3, a beam splitter creates two laser beams which reach the target object from different sides but at identical angles of incidence with equal optical path lengths. Spatial filters then scatter the laser beams, and a CCD camera records the optimal interference images which undergo computer processing and produce vibration interference data.

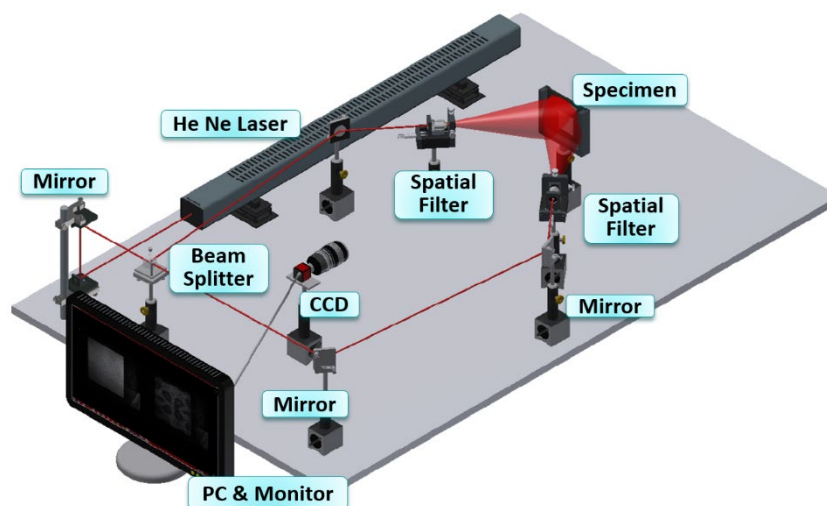


Figure 3. In-plane setup in electronic speckle pattern interferometry (ESPI).

4. Finite Element Method

We used the commercial software ABAQUS to perform finite element method (FEM) analysis calculations. For the material constants, we used the calculation results obtained using RM and the parameters provided by manufacturers and literature. It is noted that errors of about 6%-30% are produced on the natural frequencies of the first three modes, when the element used only one-layer

thickness or the linear element is applied on the perturbation. To enhance the accuracy of the numerical calculation results and to confirm the convergence in calculation, we used high-order three-dimensional 20-node piezoelectric coupling elements with reduced integration (C3D20RE). The grid size was 1 mm in the length and width directions and was divided into five equal parts along the depth, resulting in 10,580 hexahedral elements comprising 50,243 nodes. We then compared the out-of-plane and in-plane mode shapes of the piezoelectric materials using FEM with experiment measurements to verify the accuracy of the material constants.

5. Results in Material Constants

The values required for RM were measured using an impedance analyzer and then converted. With the APC-855 material as an example, we took the average of the results from the five specimens. Table 2 presents the resonant and anti-resonant frequencies measured by the impedance analyzer in the TE mode, which were substituted into Equations (7) through (10) to derive K_t , C_{33}^E , and C_{33}^D . Table 3 presents the resonant and anti-resonant frequencies measured by the impedance analyzer in the TS mode, which were substituted into Equations (12) through (16) to derive K_{15} , C_{44}^E , and C_{44}^D . Table 4 shows the capacitance values measured at 1 kHz in the TE and TS modes, which were substituted into Equations (10), (11), (17), and (18) to derive ϵ_{33}^T and ϵ_{11}^T . Table 5 displays the resonant and anti-resonant frequencies measured by the impedance analyzer in the LE mode, which were substituted into Equations (19) through (21) to derive K_{33} , S_{33}^E , and S_{33}^D . Table 6 contains the resonant and anti-resonant frequencies measured by the impedance analyzer in the LTE mode, which were substituted into Equations (22) through (24) to derive K_{31} , S_{11}^E , and S_{11}^D . Table 7 shows the resonant and anti-resonant frequencies measured by the impedance analyzer in the RAD mode, which were substituted into Equations (25) through (27) to derive K_p and σ^E .

Table 2. Resonant and anti-resonant frequencies and the converted material constants in thickness extension (TE) mode.

TE Mode	f_r (kHz)	f_a (kHz)	k_t	$c_{33}^E (\times 10^{10} N/m^2)$	$c_{33}^D (\times 10^{10} N/m^2)$
Sample 1	1205	1875	0.7967	5.7156	15.6476
Sample 2	1162.5	1857.5	0.8093	5.2983	15.3568
Sample 3	1170	1875	0.8107	5.2763	15.3900
Sample 4	1190	1855	0.7976	5.5726	15.3155
Sample 5	1182.5	1850	0.8007	5.4972	15.2331
Avg. Value	–	–	0.8030	5.4720	15.3886

Table 3. Resonant and anti-resonant frequencies and the converted material constants in thickness shear extension (TS) mode.

TS Mode	f_r (kHz)	f_a (kHz)	k_{15}	$c_{44}^E (\times 10^{10} N/m^2)$	$c_{44}^D (\times 10^{10} N/m^2)$
Sample 1	1735	2100	0.6028	2.3078	3.6251
Sample 2	1720	2045	0.5804	2.2797	3.4377
Sample 3	1720	2055	0.5867	2.2765	3.4714
Sample 4	1760	2062.5	0.5607	2.3974	3.4968
Sample 5	1745	2092.5	0.5913	2.3407	3.5992
Avg. Value	–	–	0.5844	2.3204	3.5260

Table 4. Capacitance and dielectric constant measured at 1 kHz in TE and TS mode.

TE Mode	C_T (nF)	$\epsilon_{33}^T (\times 10^{-9} F/m)$	TS Mode	C_L (nF)	$\epsilon_{11}^T (\times 10^{-9} F/m)$
Sample 1	49.0810	28.1089	Sample 1	4.7493	30.9323
Sample 2	52.4846	29.9669	Sample 2	4.7647	31.0326
Sample 3	52.7355	29.9197	Sample 3	4.8435	31.4987
Sample 4	52.3802	29.8813	Sample 4	4.2233	27.5341
Sample 5	50.9098	29.1944	Sample 5	4.2036	27.3714
Avg. Value	–	29.4142	Avg. Value	–	29.6738

Table 5. Resonant and anti-resonant frequencies and the converted material constants in length extension (LE) mode.

LE Mode	f_r (kHz)	f_a (kHz)	k_{33}	$S_{33}^E (\times 10^{-12} m^2/N)$	$S_{33}^D (\times 10^{-12} m^2/N)$
Sample 1	132.75	170	0.6631	20.1927	11.3143
Sample 2	130	163.5	0.6453	20.9192	12.2074
Sample 3	134.5	169.25	0.6459	19.4678	11.3468
Sample 4	128.5	170.5	0.6946	21.7746	11.2705
Sample 5	133	172.5	0.6749	20.0189	10.9016
Avg. Value	–	–	0.6648	20.4746	11.4081

Table 6. Resonant and anti-resonant frequencies and the converted material constants in length thickness extension (LTE) mode.

LTE Mode	f_r (kHz)	f_a (kHz)	k_{31}	$S_{11}^E (\times 10^{-12} m^2/N)$	$S_{11}^D (\times 10^{-12} m^2/N)$
Sample 1	47.6	51.05	0.4019	14.2670	11.9626
Sample 2	47.75	50.9	0.3851	14.0978	12.0070
Sample 3	48.05	51.05	0.3756	14.1336	12.1402
Sample 4	47.6	50.6	0.3772	14.3118	12.2758
Sample 5	47.15	50.75	0.4114	14.4951	12.0416
Avg. Value	–	–	0.3902	14.2611	12.0854

Table 7. Resonant and anti-resonant frequencies and the converted material constants in radial extension (RAD) mode.

RAD Mode	f_1^r (kHz)	f_1^a (kHz)	f_2^r (kHz)	f_2^r/f_1^r	k_p	σ^E
Sample 1	100.35	121.8	269.2	2.6826	0.6365	0.2296
Sample 2	100.35	121.25	268.1	2.6716	0.6312	0.2439
Sample 3	100.35	121.8	269.2	2.6826	0.6365	0.2296
Sample 4	100.35	121.25	269.2	2.6826	0.6303	0.2296
Sample 5	100.9	119.6	266.45	2.6407	0.6100	0.2856
Avg. Value	–	–	–	–	0.6289	0.2437

Table 8 compares the material constants obtained using RM and those provided by the manufacturer for piezoelectric material APC-855 from APC International, Ltd., and Table 9 compares the material constants for piezoelectric material C-2 from the Fuji Ceramics Corporation. Some differences exist between the material constants obtained using RM in this study and those provided by the manufacturer or in literature for the two piezoelectric ceramic materials. Although the difference is not very large in piezoelectric *d*-form parameters, the finite element analysis produces calculating inaccuracy or it cannot obtain the results because of the missing terms in the manufacturer provided one. Due to transformation in calculation, the *e*-form parameters in the manufacturer provided one have a larger difference with those obtained by the resonance method in this study. We therefore also substituted these material constants into FEM to calculate the high-frequency in-plane low-frequency out-of-plane

vibration characteristics and performed experimental measurements to determine the accuracy of applying these material constants to dynamic analysis.

Table 8. Material constant of APC-855 by resonance method, manufacturer, and Ref [27].

<i>d</i> Form	RM	Manufacturer Provided	<i>e</i> Form	RM	Ref [27]
Elastic compliance in constant electric field ($\times 10^{-12}$ m ² /N)			Elastic stiffness in constant electric field ($\times 10^{10}$ N/m ²)		
s_{11}^E	14.261	16.295	C_{11}^E	8.089	12.18
s_{12}^E	-3.475	-	C_{12}^E	2.451	8.021
s_{13}^E	-3.645	-	C_{13}^E	1.876	8.527
s_{33}^E	20.475	23.518	C_{33}^E	5.552	11.644
s_{44}^E	43.096	-	C_{44}^E	2.320	2.299
s_{66}^E	35.473	-	C_{66}^E	2.819	2.080
Piezoelectric strain constant ($\times 10^{-12}$ C/N)			Piezoelectric stress constant (C/m ²)		
d_{15}	661	720	e_{15}	15.338	14.26
d_{31}	-253	-276	e_{31}	-16.984	-10.48
d_{33}	516	630	e_{33}	19.156	16.60
Dielectric constant in constant stress ($\times 10^{-9}$ F/m)			Dielectric constant in constant strain ($\times 10^{-9}$ F/m)		
ϵ_{11}^T	29.674	-	ϵ_{11}^S	19.536	24.082
ϵ_{33}^T	29.414	29.218	ϵ_{33}^S	10.936	23.020

Table 9. Material constant of FUJI C-2 by resonance method and manufacturer.

<i>d</i> Form	RM	Manufacturer Provided	<i>e</i> Form	RM	Manufacturer Provided
Elastic compliance in constant electric field ($\times 10^{-12}$ m ² /N)			Elastic stiffness in constant electric field ($\times 10^{10}$ N/m ²)		
s_{11}^E	12.881	14.106	C_{11}^E	12.085	7.3
s_{12}^E	-3.834	-4.232	C_{12}^E	6.102	1.848
s_{13}^E	-5.355	-5.355 *	C_{13}^E	5.638	5.638 *
s_{33}^E	18.467	18.039	C_{33}^E	8.911	5.3
s_{44}^E	43.465	45.455	C_{44}^E	2.301	2.2
s_{66}^E	33.430	36.690	C_{66}^E	2.991	2.726
Piezoelectric strain constant ($\times 10^{-12}$ C/N)			Piezoelectric stress constant (C/m ²)		
d_{15}	573	692	e_{15}	13.183	15.224
d_{31}	-150	-158	e_{31}	-9.126	-9.126 *
d_{33}	322	367	e_{33}	11.779	11.779 *
Dielectric constant in constant stress ($\times 10^{-9}$ F/m)			Dielectric constant in constant strain ($\times 10^{-9}$ F/m)		
ϵ_{11}^T	14.832	17.442	ϵ_{11}^S	7.278	6.907
ϵ_{33}^T	12.641	12.927	ϵ_{33}^S	6.112	6.112 *

* Combined calculation results from RM experimental measurements and material parameters provided by manufacturer.

6. Discussion and Verification

We used ESPI to measure the out-of-plane and in-plane vibration characteristics of piezoelectric materials. The white regions in the images were the nodal lines, and the first lines next to them show the sub-micron vibration displacements [25,26]. The resonant frequencies measured by the impedance analyzer were also listed. Next, we applied the material constants obtained using the mathematical calculations in RM to finite element analysis software (ABAQUS) to derive the out-of-plane and in-plane resonant frequencies and mode shapes. The bold black lines in the mode shape results were the nodal lines, and we compared these numerical calculation results with experimental measurements to verify the reliability of the material constants.

6.1. APC-855

The vibration verification specimen used in this study was the thin square plate in the TE mode, in which the polarization and the vibrations are oriented along the depth. For the geometric dimensions, we used $l = 46$ mm, $w = 46$ mm, and $t = 1.2$ mm in the FEM calculations and conducted experimental verification.

6.1.1. Out-Of-Plane Vibration

As shown in Figure 4, nine mode shapes were measured in the out-of-plane vibrations, reaching around 10 kHz. “RM” indicates the results of inputting the parameters derived using RM into FEM calculations, and “Ref [27]” indicates the analysis results obtained in literature for APC-855. The simulation results of these two sets of material constants were both consistent with the mode shapes measured in the piezoelectric specimen experiments. However, the RM calculation results for the resonant frequencies were precise, the errors remaining within 6.472%. The errors in Ref [27], on the other hand, were all greater than 10% and increased as the frequency increased. This demonstrates that the material constants obtained using RM in this study have a certain degree of reliability.

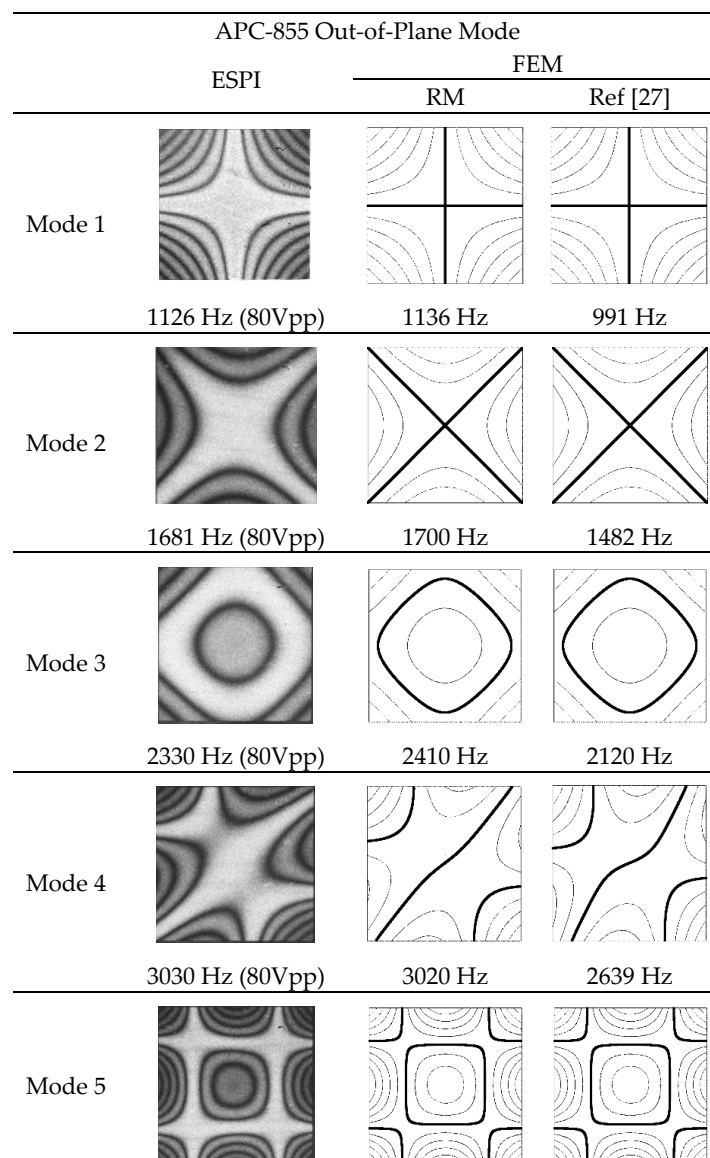


Figure 4. Cont.

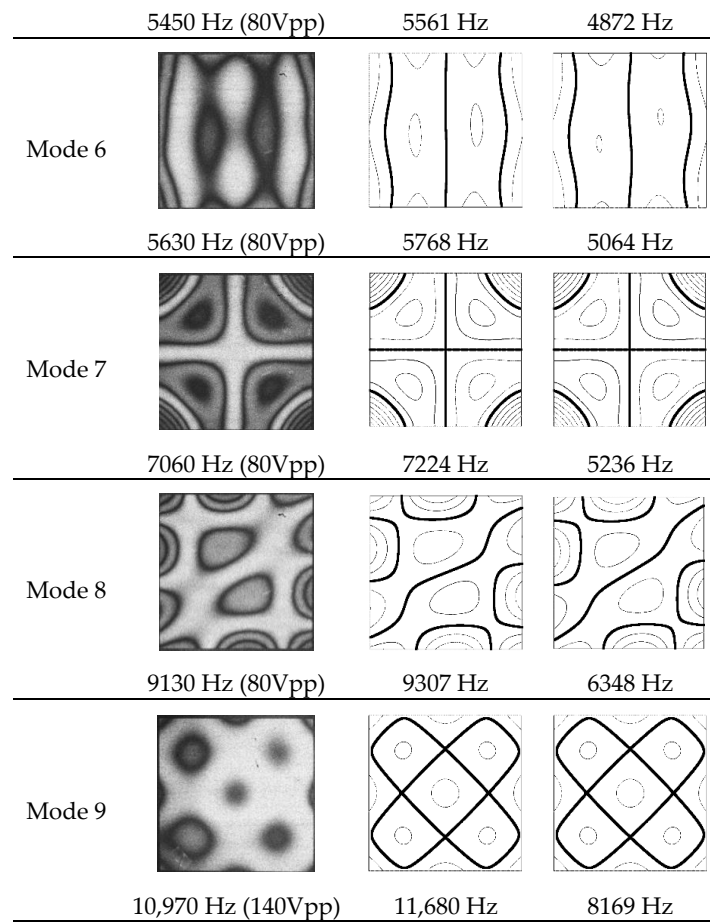


Figure 4. Out-of-plane vibration modes for APC-855.

6.1.2. In-Plane Vibration

As shown in Figure 5, five mode shapes could be obtained and the in-plane resonant frequency was in the high-frequency range from 20 kHz to 100 kHz. Mode shapes could be obtained via mode shape analysis of the material parameters derived in RM and Ref [27]. A comparison of the resonant frequency measurement results of impedance analysis and the ESPI frequency measurements revealed that they were almost identical. However, we found that the error between the RM analysis results and ESPI measurements increased as the frequency increased and exceeded 10%. In contrast, the analysis results in Ref [27] were relatively accurate. We speculate that this is because the impedance is smallest at resonant frequency vibrations; however, ESPI measurement of in-plane vibrations requires high voltages for excitation, which generates a self-heating effect and material property changes during resonance. We therefore speculate that the material constants derived in Ref [27] are better suited to the prediction of the in-plane vibrations in APC-855 following the self-heating effect. We explain this phenomenon in further detail in the following section.

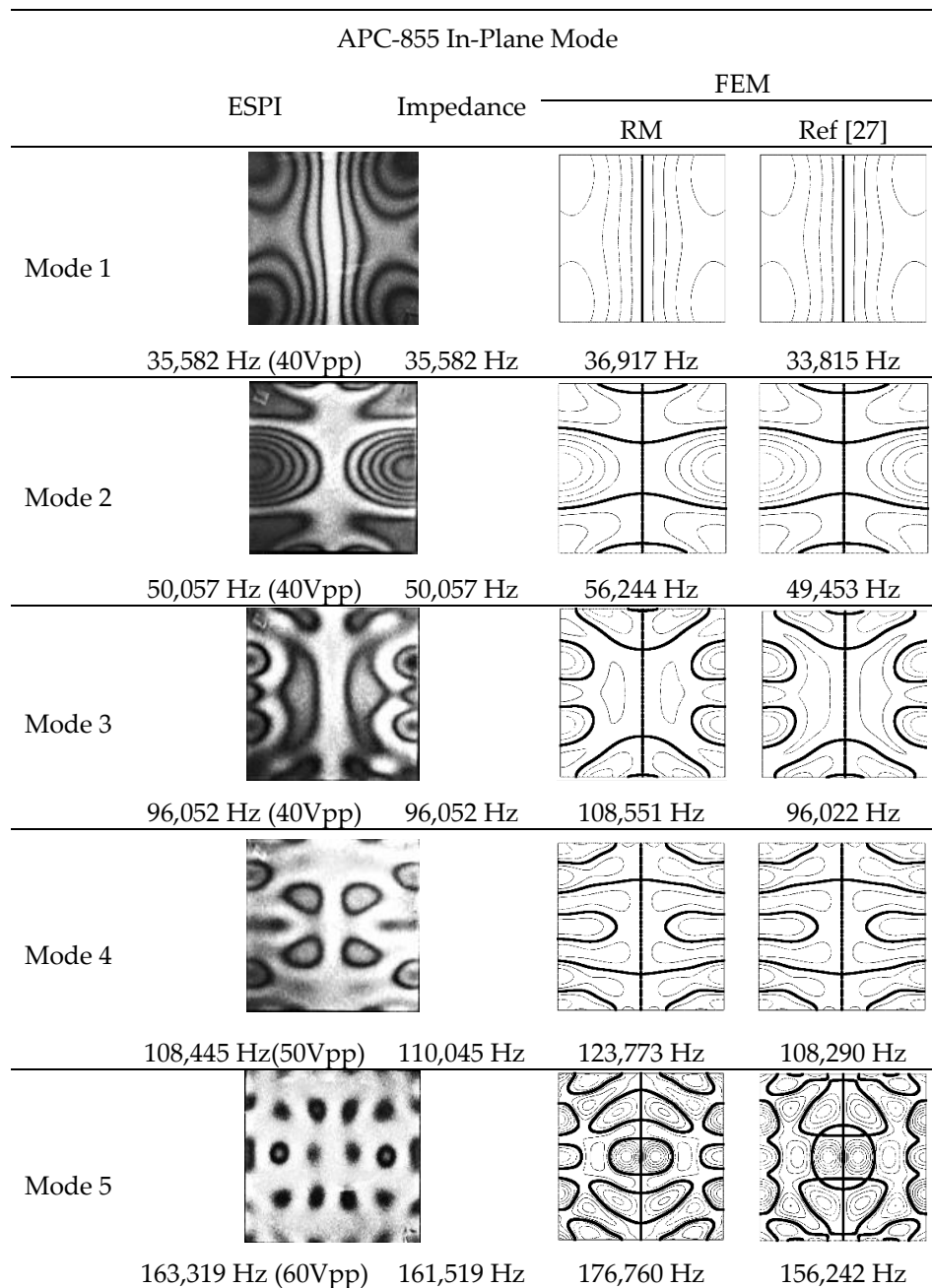


Figure 5. In-plane vibration modes for APC-855, after self heating in resonance.

6.1.3. Influence on Self-Heating in Resonance

For the out-of-plane modes, the piezoceramics was operated at lower frequencies and excited on almost one-hundred voltages. The piezoelectric material remained at almost the same temperature, which was measured by thermography at room temperature. However, we speculate that the in-plane parameters in Ref [27] are more accurate than the material constants obtained using RM in this study because APC-855 is a soft piezoelectric ceramic that is more prone to self-heating at high in-plane resonant frequencies. Thus, we used new specimens to conduct the in-plane vibration measurements. A comparison of Figures 5 and 6 show that the main difference lies in the duration of excitation. In Figure 6, the in-plane vibrations in the experiment were controlled so as to prevent self-heating caused by over-excitation [28,29]. The lower impedance occurs at the resonant frequency. The experimental measurement of in-plane vibrations requires higher excitation voltage, since ESPI

measurement is sub-micrometer resolution. Under high-voltage, high-frequency, and low-impedance excitation conditions, high temperatures are often generated in piezoelectric components, and the material properties of piezoelectric components change at high temperatures, which may alter the capacitance and material rigidity of piezoelectric ceramic. The results in Tables 5 and 6 show that after self-heating, the errors between the resonant frequency measurements of APC-855 and the results of FEM calculations using the material constants obtained with RM become significant. When the voltage and excitation time are controlled under only several seconds to confirm slight temperature rising, the resonant frequencies from the experimental ESPI measurements and impedance analysis compared to FEM are almost identical. The RM results also become accurate, with errors less than 5.314%. This verifies that the parameters measured using RM can also be used to calculate in-plane vibration values with accuracy. The errors of the Ref [27] parameters input into FEM instead become higher than they were before the self-heating of the specimen, ranging from 7% to 11%. From Equations (1) through (4), the electro-thermal-elastic model illustrated that the physical parameters and material constants were influenced by a thermal effect. In the experimental results, it is concluded that material constants and dynamic characteristics of the piezoelectric material depend on temperature. Zhang et al. [22] also show the influence on dielectric loss, dielectric constant, shifting resonant frequency of piezoelectric material through the thermal effect in their results. Hence, the RM used in the measurement of piezoelectric material constants has to be considerate of the temperature dependency in the actual application. This study therefore demonstrated that the material constants obtained using RM can be used to accurately calculate the out-of-plane and in-plane vibration characteristics of piezoelectric materials. However, the impact of self-heating must be taken into account.

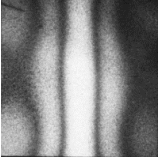
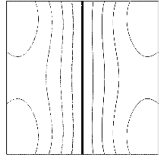
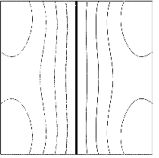
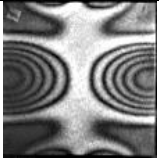
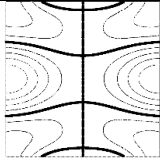
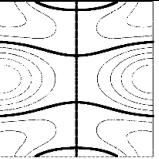
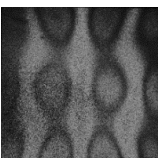
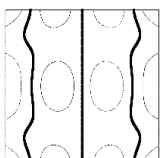
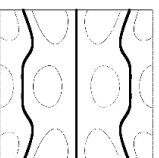
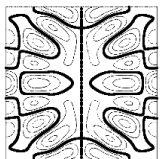
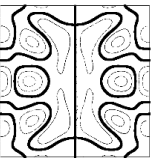
APC-855 In-Plane Mode				
	ESPI	Impedance	FEM	
			RM	Ref [27]
Mode 1				
	36,370 Hz (40Vpp)	36,370 Hz	36,917 Hz	33,815 Hz
Mode 2				
	55,554 Hz (100Vpp)	55,554 Hz	56,244 Hz	49,453 Hz
Mode 3				
	101,715 Hz (70Vpp)	101,715 Hz	101,546 Hz	92,714 Hz
Mode 4				
	168,400 Hz (140Vpp)	168,400 Hz	177,348 Hz	156,305 Hz

Figure 6. In-plane vibration mode for APC-855 before self heating in resonance.

6.2. FUJI C-2

In this paper, we discuss the accuracy of using RM to measure material constants of piezoelectric material APC-855, which is a soft ceramic in which self-heating is more severe during in-plane vibrations. We also examined the accuracy of using RM to measure material constants of piezoelectric material FUJI C-2, which is a hard ceramic. The dimensions of the test specimen were identical to those of the APC-855 specimen.

6.2.1. Out-of-Plane Vibration

As shown in Figure 7, ten mode shapes were obtained in the out-of-plane vibrations up to 12 kHz. We compared the experiment results and the FEM results. “Manufacturer provided” indicates the results of FEM calculations using the material constants provided by the manufacturer. However, not all of the parameters were available from the manufacturer, so we had to use parameters measured using RM to make up for the missing C_{13}^E , e_{31} , e_{33} , and ϵ_{33}^S in the FEM calculations of the vibration characteristics. Comparisons of the out-of-plane mode shape revealed high accuracy in all modes except Mode 5, which could not be derived using the parameters provided by the manufacturer. The RM errors were all less than 3.765%, thereby indicating that the RM results were all highly accurate. In contrast, only the errors of the results from the parameters provided by the manufacturer in Modes 1, 2, 3 and 6 were less than 10%. The errors in the remaining modes were greater than 10%. The manufacturers provided their piezoelectric material constants by measured in standard specimens; however, the quality control in turns of mass production influenced the difference of material properties. We can thus confirm that this study successfully used RM to obtain reliable material constants for piezoelectric ceramic materials.

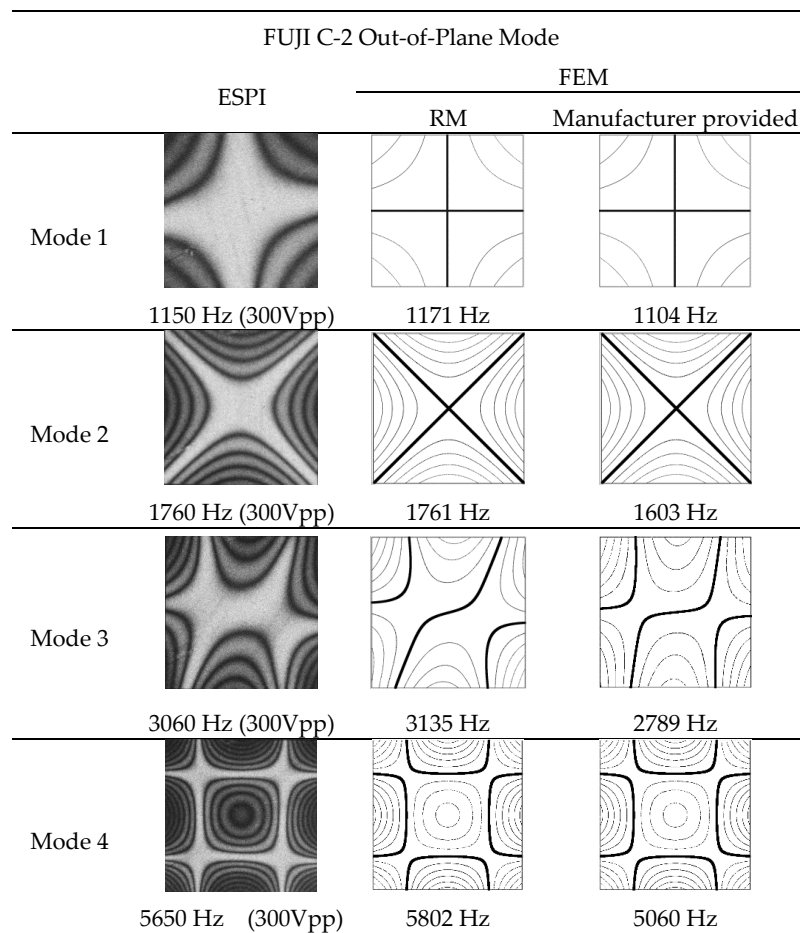


Figure 7. Cont.

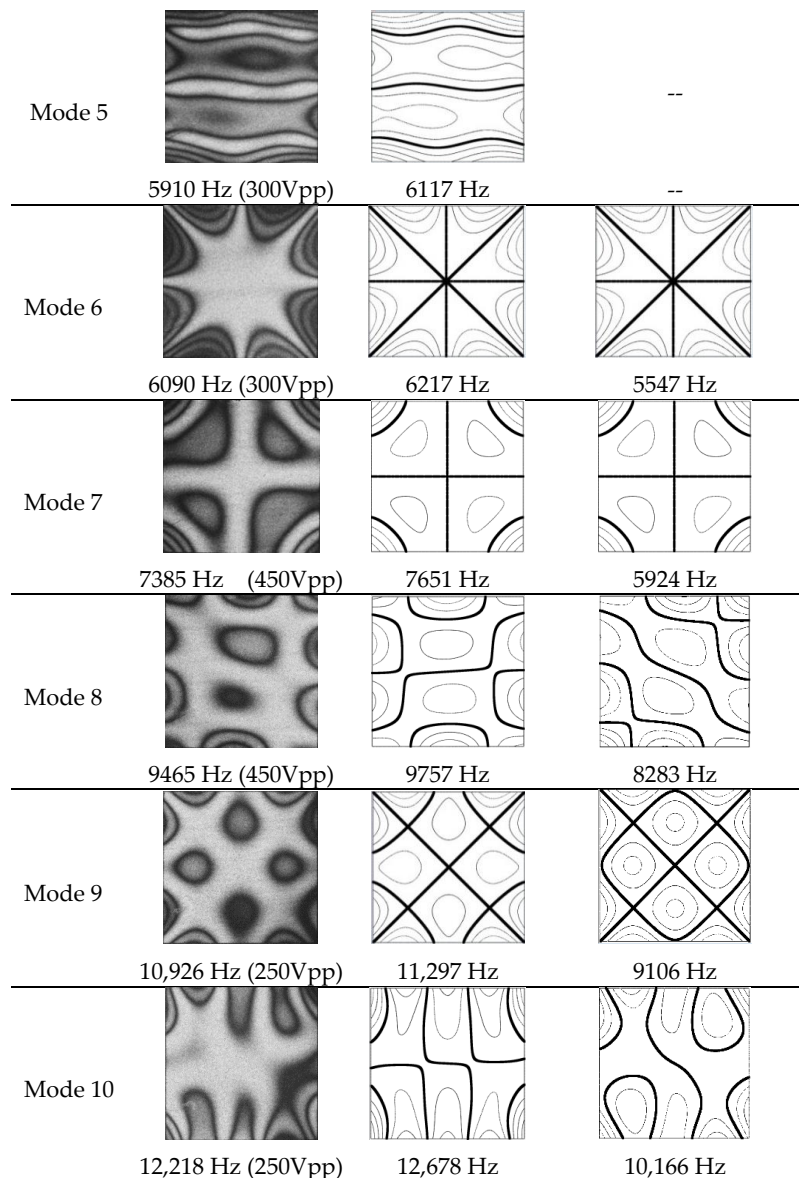


Figure 7. Out-of-plane vibration modes for FUJI C-2.

6.2.2. In-Plane Vibration

As shown in Figure 8, five mode shapes were obtained in the in-plane vibration experiments. The FEM results from RM material constants were all relatively accurate, whereas the parameters provided by the manufacturer could not produce any results at all. Because finite element analysis inputs the *e*-form material constants to calculate the results, it causes the transferred *e*-form material constants to have a larger difference with those that are manufacturer provided, as listed in Table 9. The impedance analysis results were also relatively consistent with the ESPI measurements, with only slight errors in Mode 5. The errors of the FEM calculations from the RM parameters were all within 4%, thereby indicating that the piezoelectric ceramic material constants obtained in this study were relatively reliable.

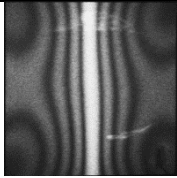
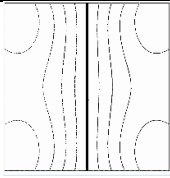
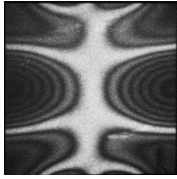
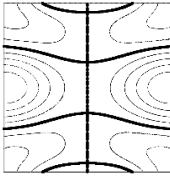
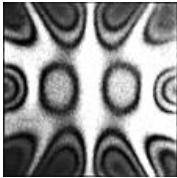
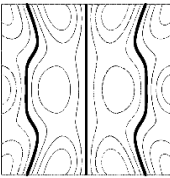
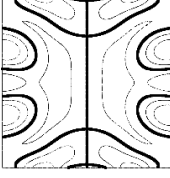
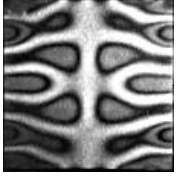
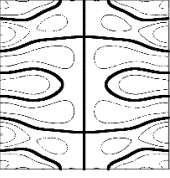
FUJI C-2 In-Plane Mode				
	ESPI	Impedance	FEM	
			RM	Manufacturer provided
Mode 1				
	38,468 Hz (40Vpp)	38,468 Hz	39,965 Hz	--
Mode 2				
	57,053 Hz (40Vpp)	57,053 Hz	58,515 Hz	--
Mode 3				
	106,212 Hz (40Vpp)	106,212 Hz	109,661 Hz	--
Mode 4				
	111,008 Hz (60Vpp)	111,008 Hz	113,614 Hz	--
Mode 5				
	123,500 Hz (40Vpp)	125,600 Hz	128,157 Hz	--

Figure 8. In-plane vibration modes for FUJI C-2.

6.3. Discussion on APC-855 and FUJI C-2

APC-855 and FUJI C-2 are soft and hard piezoelectric ceramics, respectively, and the applications of the piezoelectric effects of soft and hard piezoelectric ceramics differ. Soft piezoelectric ceramics present stronger direct piezoelectric effects and are thus more suitable for sensors, whereas hard piezoelectric ceramics show more distinct inverse piezoelectric effects and are thus more suitable for actuators. We examined the vibration measurements of these two materials via the drive voltage, and found that lower voltages can be applied to FUJI C-2 than to APC-855 while still producing ESPI measurement results at the sub-micro level. This verifies that actuators comprising hard ceramic piezoelectric materials may have stronger inverse piezoelectric effects. In contrast, soft ceramic piezoelectric materials require

greater drive voltages to make the vibration fringes clear enough to observe, but the self-heating issue severely affects the resonant frequency measurement results. Once the temperature reaches half of the Curie Temperature and remains there, thermal deterioration takes place in the material and is accompanied by depolarization [30–33]. The vibration characteristics of the piezoelectric material are also affected, thereby affecting the accuracy of material constants derived using RM. Thus, this study successfully used dynamic characteristic measurement to verify the applicability of material constants obtained using RM.

7. Conclusions

Due to the anisotropic mechanical properties of piezoelectric materials, their material constants cannot be obtained using general material testing methods. Literature indicates that RM, an approach developed over years of research using structural and polarization characteristics, can effectively measure the anisotropic parameters of piezoelectric materials. This study contains complete details on the specimens and all of the equations that should be prepared, and we used dynamic experiments to verify the accuracy of the material constants that were obtained.

RM measurements require TE, LE, TS, LTE, and RAD mode specimens. Using impedance analysis, their resonant and anti-resonant frequencies were obtained and then substituted into the RM equations. We also used the conversational relationships in constitutive equations to obtain the complete elastic, piezoelectric, and dielectric coefficients of piezoelectric ceramic materials.

We used a non-destructive testing method for dynamic characteristic measurement, verifying FEM analysis results from anisotropic material constants obtained using RM from soft and hard piezoelectric ceramic materials. The errors between the out-of-plane and in-plane mode shapes, which is frequency-dependent on material constants, derived from the RM material constants and those measured in experiments, were very small. We also discussed the impact of the temperature changes caused by self-heating in soft and hard piezoelectric ceramics on the properties of the piezoelectric materials. Whether the piezoelectric ceramic is prone to self-heating affects the accuracy of RM material constants. The dynamic analysis of non-destructive testing revealed that soft ceramic is more prone to self-heating, which shifts the original resonant frequency. This indicates that the question of whether the properties of piezoelectric materials change due to self-heating must be noted, which will in turn affect the original operating frequency and voltage designs used in transducers.

Author Contributions: This study was initiated and designed by Y.-H.H., set-up experimental platform and conducted the experiments by C.-Y.Y. and T.-R.H. T.-R.H. were also responsible in numerical simulations. C.-Y.Y. and Y.-H.H. wrote the paper. All authors contributed in analyzing the simulation and experimental results. All authors have read and agreed to the published version of the manuscript.

Funding: This research was funded by Ministry of Science and Technology (Republic of China) under Grant MOST 107-2221-E-002 -193-MY3.

Acknowledgments: The authors gratefully acknowledge the financial support of this research by the Ministry of Science and Technology (Republic of China) under Grant MOST 107-2221-E-002 -193-MY3.

Conflicts of Interest: The authors declare no conflict of interest.

Appendix A

Table A1 is listed in the material property provided by APC International, Ltd. Table A2 is listed in the material property provided by Fuji Ceramics Corporation. Table A3 is listed in the Poisson's ratio, σ^E , correspondent to the ratio of the first two resonant frequencies.

Table A1. Material constants of APC-855 piezoceramic provided from APC International, Ltd.

Item	Unit	Symbol	APC-855
Electromechanical coupling coefficient	–	k_p	0.68
		k_{33}	0.76
		k_{31}	0.40
		k_{15}	0.66
		d_{33}	630
Piezoelectric constant	$\times 10^{-12} \text{m/v}$	d_{31}	–276
Elastic constant	$\times 10^{10} \text{N/m}^2$	d_{15}	720
		C_{33}^E	5.1
		C_{11}^E	5.9
Dielectric constant	@1 kHz	$\epsilon_{33}^T / \epsilon_0$	3300
Curie temperature	$^\circ\text{C}$	T_e	200
Density	Kg/m^3	ρ	7600

Table A2. Material constants of APC-855 piezoceramic provided from Fuji Ceramics Corporation.

Item	Unit	Symbol	FUJI C-2
Electromechanical coupling coefficient	–	k_p	0.63
		k_{33}	0.76
		k_{31}	0.37
		k_{15}	0.77
		k_t	0.52
Piezoelectric constant	$\times 10^{-12} \text{m/v}$	d_{33}	367
		d_{31}	–158
		d_{15}	692
Elastic constant	$\times 10^{10} \text{N/m}^2$	C_{33}^E	5.3
		C_{11}^E	7.3
		C_{55}^E	2.2
Dielectric constant	@1 kHz	$\epsilon_{33}^T / \epsilon_0$	1460
Curie temperature	$^\circ\text{C}$	$\epsilon_{11}^T / \epsilon_0$	1970
Density	Kg/m^3	T_c	300
Poisson’s ratio	–	ρ	7600
		σ	0.3

Table A3. Poisson’s ratio corresponds to the ratio of the first two resonant frequencies.

σ^E	η_1	η_2	f_2^r/f_1^r	σ^E	η_1	η_2	f_2^r/f_1^r
0.00	1.8412	5.3314	2.8956	0.26	2.0236	5.3817	2.6595
0.01	1.8489	5.3334	2.8846	0.27	2.0300	5.3836	2.6520
0.02	1.8565	5.3353	2.8738	0.28	2.0363	5.3855	2.6447
0.03	1.8641	5.3372	2.8632	0.29	2.0426	5.3874	2.6375
0.04	1.8716	5.3392	2.8527	0.30	2.0489	5.3894	2.6304
0.05	1.8790	5.3411	2.8425	0.31	2.0551	5.3913	2.6234
0.06	1.8864	5.3431	2.8324	0.32	2.0612	5.3932	2.6165
0.07	1.8937	5.3450	2.8225	0.33	2.0674	5.3951	2.6096
0.08	1.9010	5.3469	2.8127	0.34	2.0735	5.3970	2.6028
0.09	1.9082	5.3489	2.8031	0.35	2.0795	5.3989	2.5962
0.10	1.9154	5.3508	2.7936	0.36	2.0855	5.4008	2.5897
0.11	1.9225	5.3528	2.7843	0.37	2.0915	5.4027	2.5832
0.12	1.9296	5.3547	2.7750	0.38	2.0974	5.4046	2.5768
0.13	1.9366	5.3566	2.7660	0.39	2.1033	5.4066	2.5705
0.14	1.9436	5.3586	2.7570	0.40	2.1092	5.4085	2.5642
0.15	1.9505	5.3605	2.7482	0.41	2.1150	5.4104	2.5581

Table A3. Cont.

σ^E	η_1	η_2	f_2^*/f_1^*	σ^E	η_1	η_2	f_2^*/f_1^*
0.16	1.9574	5.3624	2.7396	0.42	2.1208	5.4123	2.5520
0.17	1.9642	5.3644	2.7311	0.43	2.1266	5.4142	2.5459
0.18	1.9710	5.3663	2.7226	0.44	2.1323	5.4161	2.5400
0.19	1.9777	5.3682	2.7144	0.45	2.1380	5.4180	2.5341
0.20	1.9844	5.3701	2.7062	0.46	2.1436	5.4199	2.5284
0.21	1.9911	5.3721	2.6981	0.47	2.1492	5.4218	2.5227
0.22	1.9977	5.3740	2.6901	0.48	2.1548	5.4237	2.5170
0.23	2.0042	5.3759	2.6823	0.49	2.1604	5.4255	2.5113
0.24	2.0107	5.3778	2.6746	0.50	2.1659	5.4274	2.5058
0.25	2.0172	5.3798	2.6670				

References

- Nikkhoo, A. Investigating the behavior of smart thin beams with piezoelectric actuators under dynamic loads. *Mech. Syst. Signal Process.* **2014**, *45*, 513–530. [CrossRef]
- Kant, M.; Parameswaran, A.P. Modeling of low frequency dynamics of a smart system and its state feedback based active control. *Mech. Syst. Signal Process.* **2018**, *99*, 774–789. [CrossRef]
- Aridogan, U.; Basdogan, I.I. A review of active vibration and noise suppression of plate-like structures with piezoelectric transducers. *J. Intel. Mat. Syst. Str.* **2015**, *26*, 1455–1476. [CrossRef]
- Huang, Q.Z.; Luo, J.; Li, H.; Wang, X.H. Analysis and implementation of a structural vibration control algorithm based on an IIR adaptive filter. *Smart Mater. Struct.* **2013**, *22*, 085008. [CrossRef]
- Ru, C.G.; Pan, P.; Chen, R.H. The development of piezo-driven tools for cellular piercing. *Appl. Sci.* **2016**, *6*, 314. [CrossRef]
- Feng, Q.; Fan, L.M.; Huo, L.S.; Song, G.B. Vibration Reduction of an existing glass window through a viscoelastic material-based retrofit. *Appl. Sci.* **2018**, *8*, 1061. [CrossRef]
- Starner, T. Human powered wearable computing. *IBM Syst. J.* **1996**, *35*, 618–629. [CrossRef]
- Roundy, S.; Wright, P.K.; Rabaey, J. A study of low level vibrations as a power source for wireless sensor nodes. *Comput. Commun.* **2003**, *26*, 1131–1144. [CrossRef]
- Amirtharajah, R.; Chandrakasan, A.P. Self-powered signal processing using vibration-based power generation. *IEEE J. Solid State Circuits* **1998**, *33*, 687–695. [CrossRef]
- Beeby, S.P.; Tudor, M.J.; White, N.M. Energy harvesting vibration sources for microsystems applications. *Meas. Sci. Technol.* **2006**, *17*, R175–R195. [CrossRef]
- Ceponis, A.; Mažeika, D.; Bakanauskas, V. Trapezoidal cantilevers with irregular cross-sections for energy harvesting systems. *Appl. Sci.* **2017**, *7*, 134. [CrossRef]
- Mason, W.P.; Jaffe, H. Methods for measuring piezoelectric, elastic, and dielectric coefficients of crystals and ceramics. *Proc. IRE* **1954**, *42*, 921–930. [CrossRef]
- IRE standards on piezoelectric crystals: Measurements of piezoelectric ceramics. *Proc. IRE.* **1961**, *49*, 1161–1169. [CrossRef]
- IEEE Standard on Piezoelectricity. ANSI/IEEE Std 176-1987. 1988. Available online: <https://ieeexplore.ieee.org/document/26560> (accessed on 23 June 2020). [CrossRef]
- Wang, J.F.; Chen, C.; Zhang, L.; Qin, Z.K. Determination of the dielectric, piezoelectric, and elastic constants of crystals in class 32. *Phys. Rev. B* **1989**, *39*, 12888–12890. [CrossRef] [PubMed]
- Cao, W.W.; Zhu, S.; Jiang, B. Analysis of shear modes in a piezoelectric vibrator. *J. Appl. Phys.* **1998**, *83*, 4415–4420. [CrossRef]
- Kitamura, T.; Kadota, M.; Kasanami, T.; Kushibiki, J.I.; Chubachi, N. Evaluation of piezoelectric ceramic substrates for ultrasonic bulk wave filters and resonators using pulse interference method. *Jpn. J. Appl. Phys.* **1994**, *33*, 3212–3216. [CrossRef]
- Kuskibiki, J.; Akashi, N.; Sannomiya, T.; Chubachi, N.; Dunn, F. VHF/UHF range bioultrasonic spectroscopy system and method. *IEEE Trans. Ultrason. Ferroelectr. Freq. Control* **1995**, *42*, 1028–1039. [CrossRef]

19. Gudur, M.S.R.; Kumon, R.E.; Zhou, Y.; Deng, C.X. High-frequency rapid B-mode ultrasound imaging for real-time monitoring of lesion formation and gas body activity during high-intensity focused ultrasound ablation. *IEEE Trans. Ultrason. Ferroelectr. Freq. Control* **2012**, *59*, 1687–1699. [CrossRef]
20. Ahmad, S.N.; Upadhyay, C.S.; Venkatesan, C. Electro-thermo-elastic formulation for the analysis of smart structures. *Smart Mater. Struct.* **2006**, *15*, 401–416. [CrossRef]
21. Meitzler, A.H.; O'Bryan, H.M.; Tiersten, H.F. Definition and measurement of radial mode coupling factors in piezoelectric ceramic materials with large variations in poisson's ratio. *IEEE Trans. Sonics Ultrason.* **1973**, *20*, 233–239. [CrossRef]
22. Zhang, S.J.; Alberta, E.F.; Eitel, R.E.; Randall, C.A.; Shrout, T.R. Elastic, piezoelectric, and dielectric characterization of modified BiScO/sub 3/-PbTiO/sub 3/ ceramics. *IEEE Trans. Ultrason. Ferroelectr. Freq. Control* **2005**, *52*, 2131–2139. [CrossRef]
23. Erhart, J.; Pulpan, P.; Pustka, M. Piezoelectric ceramic resonators. In *Topics in Mining, Metallurgy and Materials Engineering*; Springer: Berlin/Heidelberg, Germany, 2017.
24. *Guide to Dynamic Measurements of Piezoelectric Ceramics with High Electromechanical Coupling*. IEC 60483:1976. 1976. Available online: <https://webstore.iec.ch/publication/2229> (accessed on 23 June 2020).
25. Lin, Y.C.; Huang, Y.H.; Chu, K.W. Experimental and numerical investigation of resonance characteristics of novel pumping element driven by two piezoelectric bimorphs. *MDPI Appl. Sci.* **2019**, *9*, 1234. [CrossRef]
26. Huang, Y.H.; Ma, C.C. Experimental measurements and finite element analysis of the coupled vibrational characteristics of piezoelectric shells. *IEEE Trans. Ultrason. Ferroelectr. Freq. Control* **2012**, *59*, 785–798. [CrossRef] [PubMed]
27. Ma, C.C.; Chang, C.Y. Improving image-quality of interference fringes of out-of-plane vibration using temporal speckle pattern interferometry and standard deviation for piezoelectric plates. *IEEE Trans. Ultrason. Ferroelectr. Freq. Control* **2013**, *60*, 1412–1423.
28. Köhler, R.; RinderknechtInstitute, S. A phenomenological approach to temperature dependent piezo stack actuator modeling. *Sens. Actuators A Phys.* **2013**, *200*, 123–132. [CrossRef]
29. Quattrocchi, A.; Freni, F.; Montanini, R. Self-heat generation of embedded piezoceramic patches used for fabrication of smart materials. *Sens. Actuators A Phys.* **2018**, *280*, 513–520. [CrossRef]
30. Zhao, H.Y.; Hou, Y.D.; Zheng, M.P.; Yu, X.L.; Yan, X.D.; Li, L.; Zhu, M.K. Revealing the origin of thermal depolarization in piezoceramics by combined multiple in-situ techniques. *Mater. Lett.* **2019**, *236*, 633–636. [CrossRef]
31. Miclea, C.; Tanasoiu, T.; Miclea, C.F.; Amarande, L.; Cioangher, M.; Trupina, L.; Iuga, A.; Spanulescu, I.; Miclea, C.T.; David, C.; et al. Behavior of the main properties of hard and soft type piezoceramics with temperature from 2 to 600 K. In Proceedings of the CAS 2010 Proceedings (International Semiconductor Conference), Sinaia, Romania, 11–13 October 2010.
32. Liao, Q.W.; Huang, P.F.; Ana, Z.; Li, D.; Huang, H.N.; Zhang, C.H. Origin of thermal depolarization in piezoelectric ceramics. *Scr. Mater.* **2016**, *115*, 14–18. [CrossRef]
33. Bobnar, V.; Kutnjak, Z.; Levstik, A. Temperature dependence of material constants of PLZT ceramics. *J. Eur. Ceram. Soc.* **1999**, *19*, 1281–1284. [CrossRef]

